# Fair Resource Allocation Schemes for Cooperative Dynamic Free-Space Optical Networks

Abdallah S. Ghazy, Hossam A. I. Selmy, and Hossam M. H. Shalaby

***Abstract*—Free-space optics (FSO) presents a promising solution for the last-mile connectivity problem. However, adverse weather conditions like fog, rain, and snow, can significantly degrade the performance of FSO links. Thus, the implementation of reliable FSO networks becomes a significant issue. At the same implementation cost, dynamic (reconfigurable) FSO networks are more robust against severe weather conditions over static ones. In this paper, two resource allocation schemes are proposed for dynamic cooperative FSO networks. Each scheme is formulated as a multi-objective optimization problem, where capacity, reliability-fairness, average transmitted power, and bit-error rate functions are targeted. One scheme prioritizes the reliability-fairness over capacity, while the other does the opposite. The simulation results reveal that the proposed schemes are more reliable and cost efficient than traditional relayed networks, especially under severe weather conditions.**

***Index Terms*—Dynamic networks; Free space optics; Lexicographic; Lex-max-min theory; Relayed networks; Resource allocation; Weighted sum.**

## I. Introduction

Free-space optics (FSO) is a line-of-site (LOS) wireless optical communication technique that is used as a promising and feasible solution for the last-mile connectivity problem, where remote network nodes are connected to a central backbone node. With the significant development in optical technology in the past decade, more FSO links are deployed in a given service area to meet increased demands on Internet services and applications [1]. Generally, FSO replaces optical fibers when short implementation time, flexible installation, and low implementation cost are required [2]. As indicated in Fig. 1, an FSO link is used to connect different remote nodes, such as mobile base stations, telephone offices, or private networks, to a central backbone node.

Manuscript received December 7, 2015; revised June 29, 2016; accepted August 31, 2016; published October 7, 2016 (Doc. ID 255159).

A. S. Ghazy is with the Department of Electronics and Communications Engineering, Egypt-Japan University of Science and Technology (E-JUST), Alexandria 21934, Egypt (e-mail: abdallah.ghazy@ejust.edu.eg).

H. A. I. Selmy is with the National Institute of Laser Enhanced Science (NILES), Cairo University, Egypt.

H. M. H. Shalaby is with the Electrical Engineering Department, Alexandria University, Alexandria 21544, Egypt.

http://dx.doi.org/10.1364/JOCN.8.000822

In spite of the attractive features of FSO, it suffers from free-space channel impairments in the infrared (IR) band spectrum, which are weather conditions, background radiation, and atmospheric turbulence [1,3,4]. Weather conditions include fog, rain, and snow that can absorb and scatter the transmitted optical signal [5]. On the other hand, eye safety regulation restricts the amount of average transmitted optical power to a certain threshold, which, in turn, limits the performance and distance of FSO links. To overcome these limitations, suitable network topologies are being investigated to provide the required quality of service (QoS) for different FSO nodes.

A conventional FSO network implements static direct links (D-Ls) between a fiber backbone node and FSO nodes, as indicated in Fig. 2(A). Although this static topology has simple and low-cost implementation, it has the worst communication performance against severe weather conditions. To overcome this degradation, serial-relayed topology is addressed [5]. In this topology, one or more relays are inserted between far nodes and the backbone node. The relay has two optical transceivers and is located at equal distances from other nodes (optimal placement) [6], as indicated in Fig. 2(B) for partial relayed link networks (P-Ls). By increasing the number of intermediate relays between remote nodes and the backbone node, the best FSO link performance can be achieved. Obviously, this enhancement in network performance comes at a significant increase in network cost. The topology, where each node is supported by one relay, is called fully relayed links (F-Ls), as indicated in Fig. 2(C).

A more robust static FSO network is achieved by implementing mesh topology [1,7]. In this topology, redundant FSO links are used between users to keep connectivities to the backbone node as indicated in Fig. 2(D). Clearly, at given atmospheric conditions, each user selects the path that achieves the highest transmission rate at an acceptable bit-error rate. Obviously, enhancing performance of static FSO networks requires installation of a large number of redundant optical transceivers, which, in turn, raises the network cost.

Better performance can be achieved at much lower cost by implementing dynamic (reconfigurable) FSO network topologies [8]. These dynamic topologies are classified according to resource sharing into cooperative and non-cooperative topologies. In dynamic non-cooperative FSO

 

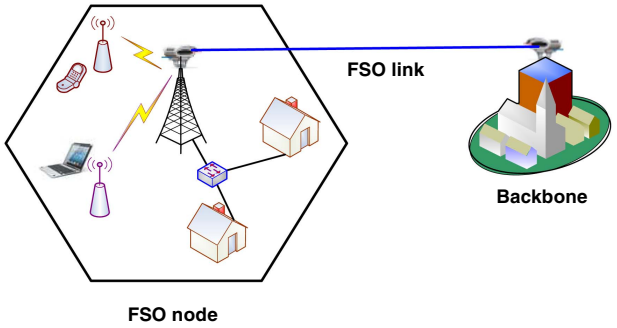


Fig. 1. Last-mile FSO connection; the end users could have wire or wireless connections to an FSO node.

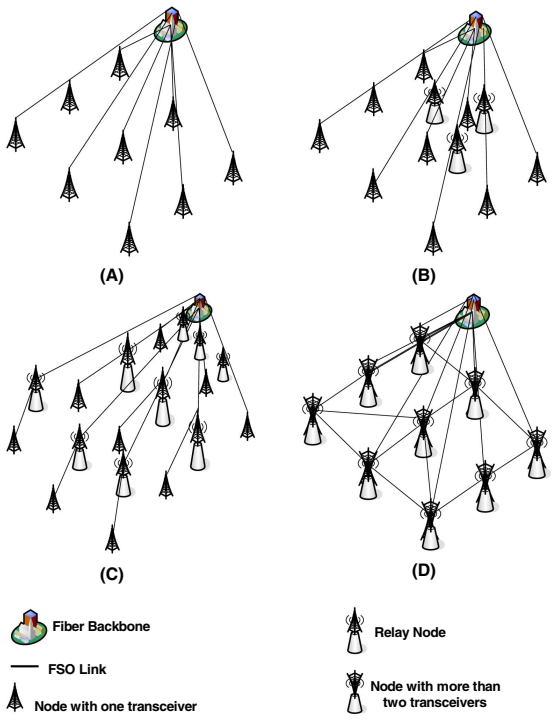


Fig. 2. FSO static topologies: (A) direct link (D-L), (B) partial relayed link (P-L), (C) full relayed link (F-L), and (D) partial mesh link.

network topologies, no resources are shared among different users [8]. Users with bad links switch their traffic to users with relatively better links and the transmission rate of each user is kept the same. This is achieved by increasing transmission rates of good links by the sum of switched rates. However, increasing the transmission rate of an optical link is not feasible and has practical limitations [3].

To cope with these limitations, dynamic cooperative topologies have been introduced. In these topologies, nodes with bad optical links switch their transmissions to nodes with better links, and the transmission rate of a good link is divided between node traffic and switched transmissions to maintain QoS for the switched ones. In other words, the network nodes cooperate and share their resources (optical bandwidths) to maintain connectivities between backbone node and far nodes under severe weather conditions. Moreover, at given weather conditions, the network resources can be fairly allocated (achieve nearly the same transmission rate as the backbone node) among different users by implementing a proper resource allocation scheme. Although the number of optical transceivers available at each node plays an important role in the network performance, it is still much lower than the number required in static topologies to achieve the same performance.

Two resource allocation schemes have recently been introduced to enhance performance of dynamic cooperative FSO networks against various weather conditions [9–11]. In this paper, the impacts of power level adaptation, operating wavelengths, and modulation techniques on the performance of these resource allocation schemes are investigated. Also, a comparison with other resource allocation schemes that use weighted sum optimization is carried out. The rest of this paper is organized as follows. Section II presents the FSO link model. Section III illustrates reconfigurable cooperative FSO network parameters. Section IV introduces the proposed resource allocation schemes. Section V shows the numerical evaluations for proposed resource allocation schemes. Last, Section VI is the conclusion and remarkable notes.

## II. FSO Link Model

Two main factors affect FSO link performance, namely, link losses and noise. Link losses include both atmospheric and geometric losses. These losses cause signal scattering, absorbing, and spreading. System noise includes both external noise (ambient or background noise) and internal noise (dark current and thermal noise). Also, the selected modulation format and wavelength play important roles in FSO link performance [12].

### A. Link Losses

FSO channel impairments have both atmospheric and geometric losses. Atmospheric loss includes fog, rain, snow, and scintillation [4]. In FSO link modeling, the collecting aperture diameter of an optical receiver may be larger than the spatial scale of the optical scintillation that is caused by atmospheric turbulence. In this condition, the FSO receiver will average fluctuations of the received waveform over the aperture area, leading to reduced signal fluctuations, especially if the network experiences weak turbulence [13–15]. In this paper, the receiver diameter is assumed to be large so that the impact of weak turbulence is small [5,16]. Under severe weather conditions, the scintillation loss has relatively small attenuation and can be neglected [5,16]. In this case, the total FSO link loss is given by

$$\gamma = \gamma_{\text{fog}} + \gamma_{\text{rain}} + \gamma_{\text{snow}_w} + \gamma_{\text{snow}_d} + \gamma_{\text{geo}}, \tag{1}$$

where $\gamma$ presents the total link loss in dB. Also, $\gamma_{\text{fog}}$, $\gamma_{\text{rain}}$, $\gamma_{\text{snow}_w}$, $\gamma_{\text{snow}_d}$, and $\gamma_{\text{geo}}$ are fog, rain, wet snow, dry snow, and geometric losses, respectively, in dB.

*1) Atmospheric Losses:* The transmission properties of optical signals in free space vary with atmospheric state.

Clearly, particles of space could absorb and scatter the transmitted optical signal. Light absorption reduces the intensity of the light beam and causes attenuation of the received optical power. Also, light scattering deflects the incident light from its initial direction, causing spatial spreading [3,4].

Fog loss is defined by several empirical models. For low-visibility ($V < 6$ km) FSO links, the Kim model is the most accurate, and is given by [1]

$$\gamma_{\text{fog}} = 10 \times \log(\exp[\beta \times L])\text{dB}, \tag{2}$$

where $\beta$ is total extinction coefficient, defined by

$$\beta = \frac{3.91}{V} \times (\lambda \backslash 550)^{-\Psi}. \tag{3}$$

Here $\Psi$ is the distribution of scattering particle size and is described by

$$\Psi = \begin{cases} 1.6; & V > 50 \text{ km}, \\ 1.3; & 6 \text{ km} < V < 50 \text{ km}, \\ 0.16 \times V + 0.34; & 1 \text{ km} < V < 6 \text{ km}, \\ V - 0.5; & 0.5 \text{ km} < V < 1 \text{ km}, \\ 0; & V < 0.5 \text{ km}, \end{cases} \tag{4}$$

where $V$ is the visibility in kilometers, $\lambda$ is the wavelength in nanometers, and $L$ is the distance in kilometers. In rainy weather, attenuation is caused by optical scattering due to droplets of water. The rain loss is calculated using Japan's empirical model [4]:

$$\gamma_{\text{rain}} = 1.58 \times D^{0.63} \times L \text{ dB}, \tag{5}$$

where $D$ is the rain fall rate in millimeters/hour (mm/h). In snowy weather, the attenuation is wavelength sensitive, but the sensitivity is not significant, so the loss is approximately equal at a wide range of wavelengths, especially with dry snow droplets.

The models below are used to calculate wet and dry snow losses [4]:

*a) Wet snow case:*

$$\gamma_{\text{snow}_w} = (1.02 \times 10^{-4}\lambda + 3.79) \times S_w^{0.72} \times L \text{ dB}, \tag{6}$$

where $S_w$ is the wet snow fall rate in mm/h.

*b) Dry snow case:*

$$\gamma_{\text{snow}_d} = (5.42 \times 10^{-5}\lambda + 5.50) \times S_d^{1.38} \times L \text{ dB}, \tag{7}$$

where $S_d$ is the dry snow fall rate in mm/h. Naturally, these weather phenomena (fog, rain, and snow) rarely occur concurrently and their influences can be studied separately [5].

*2) Geometric Loss:* Even in clear weather conditions, geometric loss is presented due to optical beam spreading through propagation in free space. This loss is calculated by [3]

$$\gamma_{geo} = 10 \times \log\left(\frac{d_t + L \times \Theta}{d_r}\right)^2 \text{dB}, \tag{8}$$

where $d_r$ is the receiver diameter, $d_t$ is the transmitter diameter (both in millimeters), and $\Theta$ is the divergence angle in mm.rad/km.

To overcome these losses and maintain network performance, an FSO link can operate with variable transmitted power and bit rate levels [17]. Obviously, in clear weather conditions, the highest transmission rate with an acceptable error rate is achieved by transmitting the lowest average power level. In contrast, during bad weather conditions, average bit-error rate is maintained by increasing the level of transmitted power and or reducing the link transmission rate. However, the maximum average transmitted power is restricted by eye safety regulations [1,3,4].

### *B. FSO System Noise*

Two kinds of noise sources are present in FSO links: thermal and shot noise. Thermal noise is generated from electronic components of the detection system, while shot noise is generated from both internal (dark current of the optical detector) and external sources (random arrival of signal and background photons). In some cases, background radiation can even cause link outage because of the saturation of the receiver, especially when the field of view (FOV) of the receiver is relatively large and/or faces a radiation source [3,4]. When the background radiation level is relatively high, the receiver thermal noise can be ignored, and the system noise is modeled using a Poisson model (shot-noise-limited receiver). Hence, at given transmitted $q_t$ photons/slot and channel loss $\gamma$, the probability of arrival of $q$ photons per slot is given by [12]

$$\text{Pos}(q, q_s + q_b) = \frac{(q_s + q_b)^q}{q!} \times \exp[-(q_s + q_b)], \tag{9}$$

where $q_s = \gamma \times q_t$ is the average number of received signal photons per slot and $q_b$ is the average number of received ambient photons per slot.

### *C. Modulation Formats*

Two prime intensity modulation/direct detection techniques, namely, non-return-zero on–off keying (NR-OOK) and pulse position modulation (PPM), are considered in this paper. PPM enhances receiver sensitivity more than OOK does, especially at high ambient noise. However, it has lower bandwidth utilization compared to OOK. The bit-error rate of OOK, $P_e$, for a shot-noise-limited receiver, is given by [12]

$$P_e = \frac{1}{2} \times \sum_{q=0}^{m_t} (q_b + q_s)^q \times \frac{\exp[-(q_b + q_s)]}{q!} + \frac{1}{2} \times \sum_{q=mt}^{\infty} (q_b)^q \times \frac{\exp[-q_b]}{q!}, \tag{10}$$

where $m_t$ is the threshold of bit detection:

$$m_t = \frac{q_s}{\log\left(1+\frac{q_s}{q_b}\right)}. \tag{11}$$

Also, the symbol-error rate of PPM, $P_s$, for a shot-noise-limited receiver, is given by [12]

$$\begin{aligned} P_s = {} & 1 - \frac{1}{M} \times \exp[(-q_s - q_b \times M)] \\ & - \sum_{q=1}^{\infty} \mathrm{Pos}(q, q_s + q_b) \times \left( \sum_{q_1=1}^{q-1} \mathrm{Pos}(q_1, q_b) \right)^{M-1} \\ & - \sum_{r=1}^{M-1} \frac{(M-1)!}{r!(M-r-1)!(r-1)} \\ & \times \sum_{q=1}^{\infty} \mathrm{Pos}(q, q_b + q_s) \times (\mathrm{Pos}(q, q_b))^r \\ & \times \left( \sum_{j=1}^{q-1} Pos(j, q_b) \right)^{M-r-1}, \end{aligned} \tag{12}$$

where $M$ is the number of slots per PPM frame. Under a constraint on the average of transmitted power, PPM outperforms multiple pulse position modulation (MPPM). In contrast, when a constraint is imposed on the peak of transmitted power, MPPM outperforms PPM [16].

The operating wavelength is an important parameter in the design of an FSO link. Indeed, it determines the impacts of geometric loss, weather attenuations, background radiation, and eye safety on FSO link performance. Generally, longer wavelengths are more immune to channel impairments than shorter ones [1,3,4]. However, in this paper, homogeneous weather is assumed over all network regions, i.e., all FSO links are affected by the same atmospheric losses and background radiation levels.

## III. Reconfigurable Cooperative FSO Network Parameters

Currently, the significant innovation in pointing, acquisition, and tracking (PAT) systems makes dynamic FSO networks more feasible than before [18]. In reconfigurable topologies, the number of FSO transceivers can be significantly reduced by replacing actual FSO relay nodes by transceivers on other working nodes (virtual FSO relay nodes) [8].

Generally, the cooperative FSO network consists of $N$ nodes $(v_1, \ldots, v_N)$ with arbitrary geographical distribution in addition to the backbone node $v_0$. The number of optical transceivers at the $k$th node is denoted by $Z_k$, where $\{k\} \in \{1, \ldots, N\}$. The backbone node is assumed to be equipped with $N$ optical transceivers. In the FSO network considered, the inner $n_2$ nodes near the backbone node are assumed to have two transceivers, while the far $n_1 = N - n_2$ nodes are assumed to have only one transceiver, i.e., $Z_k \in \{1, 2\}$. An example of a reconfigurable cooperative FSO network with one central node and nine remote nodes is shown in Fig. 3(A). In this network, each node of the inner four nodes has two transceivers ($n_2 = 4$), while each of the outer five nodes has one transceiver ($n_1 = 5$). In clear weather conditions, all nine nodes are directly connected to the central node as indicated in Fig. 3(B.1). At severe weather conditions, far nodes could switch their traffic to a neighbor node, as indicated in Fig. 3(B.2).

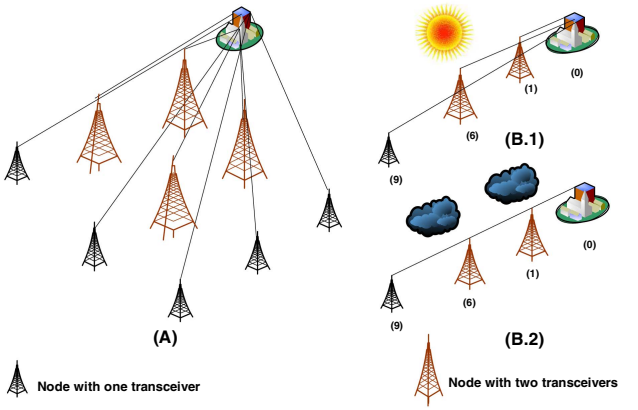


Fig. 3. Example of a reconfigurable cooperative FSO network. (A) Network topology, and network at various weather conditions: (B.1) clear weather and (B.2) foggy weather.

The losses of all FSO links are summarized in the loss matrix, $\gamma = (\gamma_{00}, \ldots, \gamma_{0N}; \ldots, \gamma_{ij}, \ldots; \gamma_{N0}, \ldots, \gamma_{NN})$, where $\gamma_{ij}$ is the loss coefficient of the FSO link between the transmitter of the $i$th node and the receiver of the $j$th node. Clearly, $0 \le \gamma_{ij} \le 1$, $\gamma_{ii} = 0$, and $\gamma_{ij} = \gamma_{ji}$ for any $\{i,j\} \in \{0, 1, \ldots, N\}$. At a given weather state, the cooperative FSO network can be connected with different feasible configurations that satisfy the required QoS parameters, i.e., guarantee minimum bit rates at bit-error rates of less than a certain threshold. The number of these feasible configurations is $\Lambda$. For the $l$th configuration, $l \in \{1, 2, \ldots, \Lambda\}$, the connection status between network nodes is summarized in connection matrix $G_l = (g_{l00}, \ldots, g_{l0N}; \ldots, g_{lij}, \ldots; g_{lN0}, \ldots, g_{lNN})$, where $g_{lij}$ is the connection status between the $i$th and $j$th nodes in configuration $l$ and $g_{lij} \in \{0, 1\}$. The connection between nodes $i$ and $j$ is established in configuration $l$ if $g_{lij} = 1$. Also, bidirectional links are assumed so that $g_{lij} = g_{lji}$ and $g_{lii} = 0$.

Clearly, the number of feasible network configurations depends on the number of transceivers on each FSO node. An upper bound for the number of feasible configurations $\Lambda$ can be obtained from the symmetric connection matrix $G_l$ with zero diagonal elements. The first row of the upper triangle of this matrix represents all connections to/from the backbone node with different $\Sigma_{i=0}^{i=N} \binom{N}{i}$ combinations. The next $n_2$ rows of the triangle represent the connections to/from all nodes that have two transceivers, resulting in $\prod_{k=1}^{k=n_2} \Sigma_{i=0}^{i=2} \binom{N-k}{i}$ different connections. The next $n_1$ rows of the triangle represent the connections to/from all nodes that have one transceiver, resulting in $\prod_{k=1}^{k=n_1} \Sigma_{i=0}^{i=1} \binom{N-n_2-k}{i}$ different connections. Therefore, the size of $\Lambda$ can be deduced by the following simple upper bound:

$$\Lambda < \sum_{i=0}^{i=N} \binom{N}{i} \times \prod_{k=1}^{k=n_2} \sum_{i=0}^{i=2} \binom{N-k}{i} \times \prod_{k=1}^{k=n_1} \sum_{i=0}^{i=1} \binom{N-n_2-k}{i}. \quad (13)$$

Moreover, all FSO links are assumed to have adaptive average transmitted power, i.e., the power of the optical link between nodes $i$ and $j$ in configuration $l$ is one of discrete values, $P_{lij} \in \{0, y_1, y_2, \ldots, y_Y\}$, and $y_1 < y_2 < \cdots < y_Y$. The average transmitted power of node $k$ in configuration $l$ is denoted by $P_{lk}$, where $P_{lk} = \Sigma_{j=0}^{N} P_{lkj}$. However, to increase link capacity and guarantee an error rate of less than a specified maximum $\text{BER}_{lij} < \text{BER}_{\max}$, the link between nodes $i$ and $j$ in configuration $l$ adapts its transmission rate, $T_{lij}$, to be one of $X+1$ discrete values, where $T_{lij} \in \{0, x_1, x_2 \ldots, x_X\}$ and $x_1 < x_2 < \cdots < x_X$. The transmission rate of node $k$ in configuration $l$ is denoted by $T_{lk}$, where $T_{lk} = \Sigma_{j=0}^{N} T_{lkj}$. The bit rate of node $k$ (its own traffic) through connection to node $j$ in configuration $l$ is denoted by $R_{lkj}$. The overall bit rate of node $k$ in configuration $l$ is $R_{lk} = \Sigma_{j=0}^{N} R_{lkj}$. Obviously, $R_{lk} \le T_{lk}$, and for practical implementation both $R_{lk}$ and $T_{lk} \in \{0, x_1, x_2, \ldots, x_X\}$. The end-to-end bit-error rate of node $k$ in configuration $l$, $\text{BER}_{lk}$, is bounded by $\text{BER}_{lk} \le \text{BER}_{\max}$. The bit rates and bit-error rates associated with all nodes in the feasible configurations can be summarized in $(\Lambda \times N)$ matrices $R$ and $E$, respectively. For a given configuration $l$, the bit rates for all nodes are represented in vector $r_l$ $(1 \times N)$, $r_l \in R$. Also, the bit-error rates in that configuration are summarized in vector $e_l$ $(1 \times N)$, $e_l \in E$.

The network capacity and average transmitted power associated with configuration $l$ are given by $C_l = \Sigma_{k=1}^{N} R_{lk}$ and $P_l = \Sigma_{k=1}^{N} P_{lk}$, respectively. All capacity and power values associated with all feasible configurations are summarized in vectors $C$ $(\Lambda \times 1)$ and $P$ $(\Lambda \times 1)$, where $C_l \in C$ and $P_l \in P$. Also, the maximum network capacity that can be achieved by any configuration is that obtained from direct link configuration $l^*$ and is defined by $C_{\max} = \Sigma_{k=1}^{N} T_{l^* k0}$. Table I summarizes the assigned symbols for the FSO network parameters.

TABLE I
NETWORK PARAMETERS

| | |
|---|---|
| $v$ | Node vector $(1 \times (N+1))$ |
| $\gamma$ | Loss coefficient matrix $((N+1) \times (N+1))$ |
| $G$ | Connection matrix $((N+1) \times (N+1))$ |
| $R_{lkj}$ | Bit rate of $k$th node to node $j$ for $l$th configuration |
| $R_{lk}$ | Bit rate of $k$th node for $l$th configuration |
| $r_l$ | Bit rate vector for $l$th configuration $(1 \times N)$ |
| $R$ | Bit rate matrix $(\Lambda \times N)$ |
| $\text{BER}_{lkj}$ | Bit-error rate of $k$th node to $j$th node for $l$th configuration |
| $\text{BER}_{lk}$ | Bit-error rate of $k$th node for $l$th configuration |
| $e_l$ | Bit-error rate vector for $l$th configuration $(1 \times N)$ |
| $E$ | Bit-error rate matrix $(\Lambda \times N)$ |
| $\text{BER}_{\max}$ | Bit-error rate threshold |
| $C_l$ | Capacity of the network for $l$th configuration |
| $C$ | Capacity vector $(\Lambda \times 1)$ |
| $C_{\max}$ | Maximum capacity |
| $T_{lij}$ | Transmission rate between $i$ and $j$ nodes for $l$th configuration |
| $T_{lk}$ | Transmission rate of $k$th node for $l$th configuration |
| $Z_k$ | Number of transceivers of $k$th node |
| $P_{lij}$ | Power of $i, j$ link for $l$th configuration |

## IV. Proposed Fair Cooperative Resource Allocation Schemes

Dynamic cooperative FSO networks deploy resource allocation schemes to increase capacity, reliability, and fairness under various weather conditions. Increasing network capacity is achieved by maintaining the largest number of direct links to the central node. In addition, increasing network reliability implies decreasing the number of dropped nodes, while enhancing fairness means nearly the same bit rates are assigned to different nodes. Obviously, under clear weather conditions, all nodes are directly connected to the central node to get the highest bit rates (maximum network capacity) at bit-error rates of less than a predefined threshold, as indicated in Fig. 3(B.1). In contrast, under bad weather conditions, direct links of far nodes are dropped and switched to other nodes (according to the resource allocation scheme) to keep connectivity to the central node.

Resource allocation in a dynamic cooperative FSO network can be optimized for several performance metrics and objectives. Given a number of optical transceivers in each node (one or two transceivers in our case), the loss coefficient matrix of FSO links $\gamma$, and discrete values of transmitted power, many feasible configurations could enable the $k$th node $(k \in \{1, \ldots, N\})$ to have a bit rate $R_k \in \{0, x_1, x_2, \ldots, x_X\}$ at a bit-error rate of less than the threshold $\text{BER}_k \le \text{BER}_{\max}$. Among these feasible configurations, one or more could achieve highest network reliability, fairness, and capacity, and the lowest power and/or bit-error rate. Clearly, the optimized objective functions are conflicted, so each resource allocation scheme is presented by multiple objective optimization problems (MOOPs). There are several methods to formulate MOOPs, such as lexicographic (hierarchical), weighted sum, product, and bounded objective functions [19]. Lexicographic optimization is a criterion to optimize conflicted objectives hierarchically, and it has the ability to achieve resource allocation goals [19,20]. With the lexicographic method, the objective functions are arranged in order of importance (optimization levels), and then the objective functions are solved one at a time. On the other hand, the weighted sum scheme optimizes the objectives simultaneously by transforming the multi-objective function into one scalar objective. There are many forms by which to construct the weighted sum function; however, the simplest one is the linear form [19]. In this section, both lexicographic and weight sum optimization are used to formulate two resource allocation schemes for dynamic cooperative FSO networks. The first scheme considers the optimization of both capacity and fairness (constrained fairness), while the second one optimizes the fairness regardless of the capacity.

### A. Lexicographic Schemes

In this subsection, two resource allocation schemes are proposed to enhance the performance of dynamic

cooperative FSO networks. These schemes are proposed for FSO networks that use two optical transceivers for the inner nodes and one transceiver for the outer nodes, as indicated in Fig. 3(A). The schemes use the concept of lex-max-min fairness, which is widely used in computer and wireless networks to overcome the congestion and limited reliability of the network [21]. Lex-max-min fairness is a criterion for achieving near equal resource sharing among $N$ nodes at a relatively high network capacity, i.e., avoiding inefficient fairness (allocate the lowest bit rate $x_1$ for all nodes to achieve the maximum fairness). Lex-max-min fairness is the generalization of ordinary max-min fairness as it searches sequentially for the next maximal, in the case that two or more solutions have the same maximal at one level in the space of feasible solutions [21,22].

The first proposed scheme is called lex-max-min constrained fairness (LMMCF), which aims at enhancing network capacity while maintaining fairness between nodes. The second proposed scheme is called lex-max-min fairness (LMMF), which aims at enhancing both reliability and fairness of the network regardless of the capacity. The LMMCF scheme targets four ordered objective functions, which are maximizing network capacity, maximizing bit rate fairness, minimizing power, then finally minimizing bit-error rate. In contrast, the LMMF scheme targets three ordered objective functions, which are maximizing bit rate fairness, minimizing power, then finally minimizing bit-error rate.

*1) LMMCF:* Lexicographic optimization represents the problem in four levels of optimization based on the priorities between the objectives as

$$\underset{l}{\textbf{Max:}}\left\{C_l=\sum_{k=1}^{k=N}R_{lk}:C_l\in C\right\}$$

$$\underset{l}{\textbf{Lex-Max-Min}}\{r_l=(R_{l1},R_{l2},\ldots,R_{lN}):r_l\in R\}$$

$$\underset{l}{\textbf{Min:}}\left\{P_l=\sum_{k=1}^{k=N}P_{lk}:P_l\in P\right\}$$

$$\underset{l}{\textbf{Lex-Min-Max}}\{e_l=(\mathrm{BER}_{l1},\ldots,\mathrm{BER}_{lN}):e_l\in E\}$$

**Subject to:**

$$l\in\{1,2,3,\ldots,\Lambda\},\qquad Z_k\in\{1,2\},$$

$$R_{lk}=\sum_{j=0}^{N}R_{lkj},\qquad R_{lk}\le T_{lk},\qquad T_{lk}=\sum_{j=0}^{N}T_{lkj},$$

$$\mathrm{BER}_{lk}\le\mathrm{BER}_{\max},\qquad \mathrm{BER}_{lij}<\mathrm{BER}_{\max},$$

$$P_{lk}=\sum_{j=0}^{j=N}P_{lkj},\qquad P_{lkj}\in\{0,y_1,y_2,\ldots,y_Y\},$$

$$\{R_{lk},R_{\mathrm{lkj}},T_{lk},T_{lkj}\}\in\{0,x_1,x_2,\ldots,x_X\},$$

$$k\in\{1,2,\ldots,N\},\qquad \{i,j\}\in\{0,1,2,\ldots,N\},\qquad j\ne i. \tag{14}$$

This scheme first increases network capacity then proceeds to improve both network reliability and fairness. The network capacity is the summation of all nodes' bit rates. Also, the improvement in both reliability and fairness are raised by maximizing bit rates of the far nodes. Specifically, at the first optimization level, the LMMCF scheme selects from the feasible $\Lambda$ configurations the ones that maximize network capacity. After that, in the second optimization level, the scheme searches the previously selected configurations for the ones that maximize the minimum bit rate for all nodes.

If there are two or more configurations that have the same max-min bit rate, the LMMCF scheme proceeds to select from them the configurations that have the next max-min bit rate (sequential max-min optimization) [21]. However, if there is more than one configuration with the same sequential max-min values, the LMMCF selects from them in a third optimization level the configurations that have the lowest transmitted power. Finally, if two or more configurations have the same minimum power, the LMMCF selects from them in a fourth optimization level the configuration that minimizes the maximum bit error rates sequentially (sequential min-max optimization) [22]. In addition, only specific discrete values for bit rates, transmission rates, and power levels are allowed. In this sense, the bit rates $R_{lkj}$ associated with node $k$ are selected so that their summation $R_{lk}$ is one of the allowed discrete values. This is also applied to the transmission rate associated with each node. Moreover, the average transmitted power is variable to discrete values. Clearly, in this optimization problem, improvement in the bit rate fairness between different users is restricted by network capacity. Also, an improvement in power efficiency restricts the decreasing of the average error rate.

*2) LMMF:* Toward achieving the highest network reliability and fairness, capacity optimization is omitted when searching among the feasible configurations. The LMMF scheme selects from the feasible configurations the ones that maximize minimum bit rate for all nodes in sequential LMM optimization. However, if there is more than one feasible configuration with the same sequential LMM bit rate, the scheme proceeds to select among these configurations the ones that achieve the lowest overall transmitted power. Finally, if there is more than one solution, LMMF selects the ones that achieve the sequential LMM bit-error rates for all nodes. The scheme is presented using lexicographic optimization as three optimization levels based on the priorities between the objectives and is described as

$$\underset{l}{\textbf{Lex-Max-Min}}\{r_l=(R_{l1},R_{l2},\ldots,R_{lN}):r_l\in R\}$$

$$\underset{l}{\textbf{Min:}}\left\{P_l=\sum_{k=1}^{k=N}P_{lk}:P_l\in P\right\}$$

$$\underset{l}{\textbf{Lex-Min-Max}}\{e_l=(\mathrm{BER}_{l1},\ldots,\mathrm{BER}_{lN}):e_l\in E\}$$

**Subject to:**

$$l \in \{1,2,3,\ldots,\Lambda\}, \qquad Z_k \in \{1,2\},$$
$$R_{lk} = \sum_{j=0}^{N} R_{lkj}, \qquad R_{lk} \le T_{lk}, \qquad T_{lk} = \sum_{j=0}^{N} T_{lkj},$$
$$\mathrm{BER}_{lk} \le \mathrm{BER}_{\max}, \qquad \mathrm{BER}_{lij} < \mathrm{BER}_{\max},$$
$$P_{lk} = \sum_{j=0}^{j=N} P_{lkj}, \qquad P_{lkj} \in \{0, y_1, y_2, \ldots, y_Y\},$$
$$\{R_{lk}, R_{lkj}, T_{lk}, T_{lkj}\} \in \{0, x_1, x_2, \ldots, x_X\},$$
$$k \in \{1,2,\ldots,N\}, \qquad \{i,j\} \in \{0,1,2,\ldots,N\}, \qquad j \ne i. \tag{15}$$

Both schemes have the same optimization constraints. However, the capacity achieved by LMMCF is higher than that of LMMF, while bit rate fairness achieved in the LMMF case is better than that of LMMCF. This could be interpreted as follows. In LMMF, the $k$th node begins to switch its direct link to another indirect one if its bit rate $R_k$ starts to be less than the maximum value $x_X$. This, in turn, decreases the number of direct links in the network and consequently decreases the capacity. In contrast, for the LMMCF scheme, the node begins to switch its direct link if its bit rate $R_k$ starts to be less than the minimum allowable value $x_1$. Clearly, this employs the direct links in order to increase the capacity. In this way, network operators have the ability to select from different resource allocation schemes that provide different QoS services.

### *B. Weighted Sum Schemes*

In the lexicographic method, the improvement of the second-order objective is restricted by the optimized values of higher order objectives and, clearly, this could provide the best formulation of resource allocation in a dynamic cooperative FSO network. However, to compare with other optimization formulations, linear weighted sum functions are constructed in the form $U = \sum_i \alpha_i \times U_i$, where $\alpha_i$ are the optimization weights, $U_i$ are the optimization objectives, and $\sum_i \alpha_i = 1$. In this method, the normalized performance objectives are scaled and combined linearly. For the $l$th configuration, normalized capacity $\bar{\zeta}_l$ normalized reliability $\bar{\Re}_l$, fairness $F_l$, normalized average transmitted power $\bar{P}_l$, and normalized average error rate $\bar{\xi}_l$ are given as

$$\bar{\zeta}_l = C_l/(N \times x_X), \qquad 0 \le \bar{\zeta}_l \le 1, \tag{16}$$

$$\bar{\Re}_l = \frac{1}{N}\sum_{k=1}^{k=N} \delta_{lk}, \qquad \delta_{lk} = \begin{cases} 1 & R_{lk} > 0 \\ 0 & R_{lk} = 0 \end{cases}, \qquad 0 \le \bar{\Re}_l \le 1, \tag{17}$$

$$F_l = \left(\sum_{k=1}^{k=N} R_{lk}\right)^2 \Big/ \left(N \times \sum_{k=1}^{k=N} R_{lk}^2\right), \qquad 0 \le F_l \le 1, \tag{18}$$

$$\bar{P}_l = P_l/(\lfloor (N + n_1 + 2 \times n_2)/2 \rfloor \times y_Y), \qquad 0 \le \bar{P}_l \le 1, \tag{19}$$

$$\bar{\xi}_l = \frac{1}{C_l \times \mathrm{BER}_{\max}} \sum_{k=1}^{k=N} R_{lk}.E_{lk}, \qquad 0 \le \bar{\xi}_l \le 1. \tag{20}$$

As indicated in Eq. (18), Jain's index $F$ is used in evaluating the bit rate fairness among different $N$ nodes [23]. The weighted sum formulation of the proposed two resource allocation schemes under the same optimization constraints is given as

$$\underset{l}{\mathbf{Max}}: U_l = \alpha_1 \times \bar{\zeta}_l + \alpha_2 \times (\bar{\Re}_l + F_l)/2 - \alpha_3 \times \bar{P}_l - \alpha_4 \times \bar{\xi}_l.$$

**Subject to:**

$$l \in \{1,2,3,\ldots,\Lambda\},$$
$$R_{lk} = \sum_{j=0}^{N} R_{lkj}, \qquad R_{lk} \le T_{lk}, \qquad T_{lk} = \sum_{j=0}^{N} T_{lkj},$$
$$\mathrm{BER}_{lk} \le \mathrm{BER}_{\max}, \qquad \mathrm{BER}_{lij} < BER_{\max},$$
$$P_{lk} = \sum_{j=0}^{j=N} P_{lkj}, \qquad P_{lkj} \in \{0, y_1, y_2, \ldots, y_Y\},$$
$$k \in \{1,2,\ldots,N\}, \qquad \sum_{ii=1}^{ii=4} \alpha_{ii} = 1, Z_k \in \{1,2\},$$
$$\{R_{lk}, R_{lkj}, T_{lk}, T_{lkj}\} \in \{0, x_1, x_2, \ldots, x_X\},$$
$$\{i,j\} \in \{0,1,2,3,\ldots,N\}, \qquad j \ne i. \tag{21}$$

Clearly, increasing importance or priority of a performance object is achieved only by increasing its associated weight relative to the weights of other objectives in the optimization equation. Furthermore, using this general formulation, weighted sum constrained fairness (WSCF) could be formulated by selecting $\alpha_1 \gg \alpha_2 \gg \alpha_3 \gg \alpha_4$. With this selection, WSCF aims to give high priority to increasing network capacity and less priority to increasing bit rate fairness among different nodes, the same as in LMMCF. On the other hand, the weighted sum fairness (WSF) scheme can be formulated by selecting $\alpha_1 = 0$, $\alpha_2 \gg \alpha_3 \gg \alpha_4$, and it clearly performs like the proposed LMMF scheme.

Generally, Eqs. (14), (15), and (21) are classified as integer linear programming (ILP) multiple objective optimization problems (discrete linear MOOPs). These equations can be solved by using the exhaustive search (ES) method to obtain the optimal solution(s). In the ES method, all feasible configurations ($\beta$) are first generated using the predefined optimization constraints. After that, the configurations are evaluated for the prioritized or weighted objective functions to obtain the optimal solution(s) [24].

The computational complexity of the ES method is of the order of $O(2^N)$. In small networks ($N < 30$), ES can be performed. However, in large networks, heuristic methods and genetic algorithms (GAs) are used to obtain sub-optimal solution(s) with a reasonable number of computational operations [25]. The ES method is used to solve the two ILP-MOOPs. However, to overcome the solution complexity for the proposed schemes, the optimal solution(s) can be computed offline, then it/they can be stored in a lookup

table in an FSO tracking controller to achieve real-time allocation.

## V. Simulation and Numerical Results

In this section, both the LMMCF and LMMF resource allocation schemes are evaluated and compared to existing schemes to indicate the superior performance of the proposed schemes. The evaluations are based on five performance parameters, which are reliability, capacity, bit rate fairness, average transmitted power, and bit-error rate. These parameters are evaluated under different weather conditions, which are fog, rain, and snow. Also, some figures are introduced to indicate the performance difference between the WSCF/WSF and LMMCF/LMMF schemes in cooperative dynamic networks.

An NR-OOK format at fixed power level $P = -15$ dBm and $\lambda = 1550$ nm is assumed for most evaluations. However, the impacts of using 780 nm wavelength is demonstrated in Figs. 9 and 15. Also, NR-OOK performance is compared with that of 4-PPM ($M = 4$), as indicated in Fig. 11. Furthermore, the impact of changing transmitted power level on network performance is shown in Figs. 17 and 18.

As shown in Fig. 4, the assumed service area of the considered FSO networks is 3 km × 3 km, and nine FSO nodes are assumed to be located uniformly in this area. Moreover, the same homogeneous weather is assumed throughout the service area. Four topologies are considered in the evaluations, which are direct link (D-L) [Fig. 2(A)], partial relayed (P-L) [Fig. 2(B)], full relayed (F-L) [Fig. 2(C)], and reconfigurable cooperative [Fig. 3(A)] models. The number of transceivers used for these networks are 18, 24, 36, and 22, respectively. All FSO links operate with predefined six-bit rates, $X = 6$, at a constant average optical power. Table II shows the assigned values of the simulated FSO network parameters, which are selected to be in the practical range. From this table, the receiver diameter is $d_r = 0.2$ m, and the largest FSO link distance is $L = 3700$ m. The aperture averaging is calculated as $A = [1 + 1.33 \times (2\pi/\lambda \times d_r^2/L)]^{-7/5} = 0.0038$. Clearly, when using this value of aperture averaging, the attenuation variance caused by weak turbulence has small value and

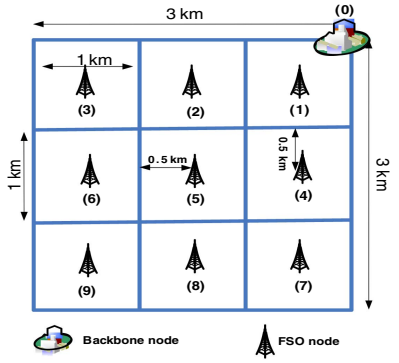


Fig. 4. Service area of simulated FSO networks.

TABLE II
Simulation Parameters

| Link Parameters | Values |
|---|---|
| Signal wavelength ($\lambda$) | 1550 nm |
| Divergence angle ($\Theta$) | 2 mm.rad/m |
| Diameter of transmitter ($d_t$) | 4 cm |
| Diameter of receiver ($d_r$) | 20 cm |
| Average transmitted signal counts/slot ($q_t = q_s/\gamma$) | 250,000 |
| Average background counts/slot ($q_b$) | 50 |
| Average transmitted power ($P$) | −15 dBm |
| Average background noise power | −52 dBm |
| Discrete bit rates ($\{x_X, \ldots, x_2, x_1\}$) in Gbps | 1, 3/4, 2/3, 1/2, 1/3, 1/4 |
| Modulation format | NR-OOK |
| BER threshold ($BER_{max}$) | $10^{-4}$ |
| Area of FSO network | 3 km × 3 km |
| Area of FSO node cell | 1 km × 1 km |

can be neglected [14]. Generally, including attenuation caused by weak or strong scintillations will not change the problem formulation of the proposed resource allocation schemes, and it could be directly added to other attenuations in the channel loss matrix $\gamma$.

Figures 5–9 demonstrate low-visibility atmosphere (fog, low clouds, dust, smoke, etc.) impacts on the considered network performance.

Figure 5 indicates the reliability of the topologies versus visibility. Clearly, at $V \geq 2.8$ km, the nine nodes for all topologies work properly using their direct FSO links. In contrast, at $V \leq 200$ m all nodes for all topologies are dropped, i.e., cannot achieve the minimum bit rate (0.25 Gbps) at a bit-error rate of less than threshold ($10^{-4}$). Between these two visibility levels, different network topologies have different performance. At $V = 1.4$ km, six, three, and two nodes are dropped in D-L, P-L, and LMMF/LMMCF, respectively. Although LMMF and LMMCF have identical performance curves, in general the reliability of LMMF is better than that of LMMCF due to its flexibility in link reconfiguration (no capacity constraint).

Figure 6 shows the capacity of the networks where the capacity is 9 Gbps for all topologies at $V \geq 3.8$ km, and zero

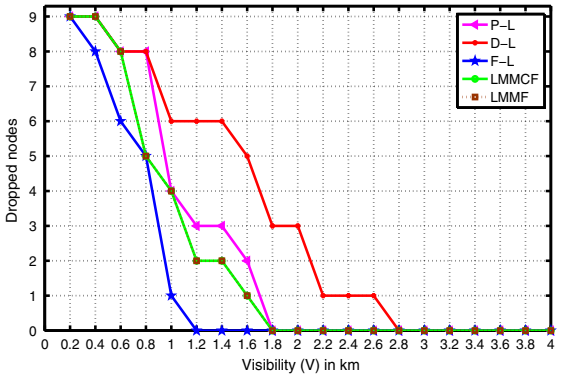


Fig. 5. Network reliability presented in number of dropped nodes versus visibility ($V$) for D-L, P-L, F-L, LMMCF, and LMMF networks.

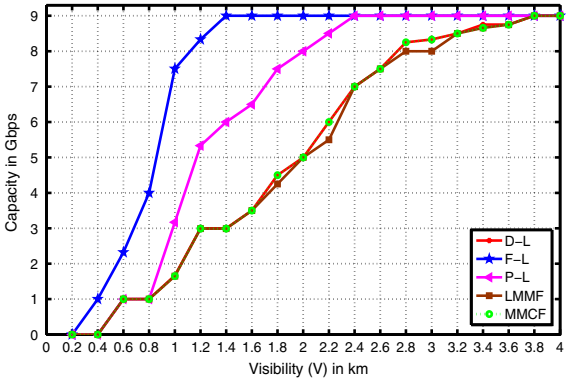


Fig. 6. Capacity versus visibility ($V$) for D-L, F-L, P-L, LMMF, and LMMCF networks.

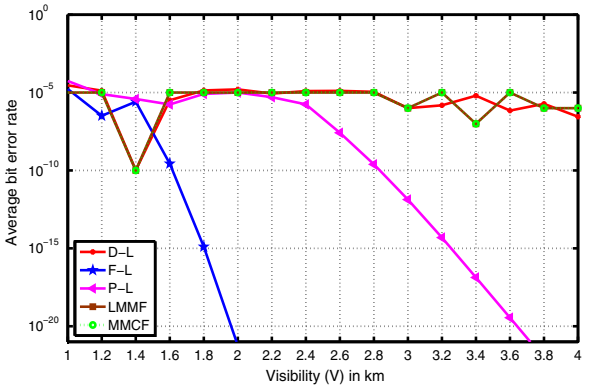


Fig. 8. Bit-error rate (BER) versus the visibility ($V$) for D-L, F-L, P-L, LMMF, and LMMCF networks.

at $V \leq 200$ m. Also, F-L is still the best topology, and then P-L, since the average transmitted power in these topologies is higher than in other topologies. The performance of the other three topologies is almost the same; however, the D-L and LMMCF topologies are better than LMMF at certain $V$ values, as expected. Numerically, at $V = 2.2$ km the capacities of D-L and LMMCF are 6 Gbps ($= C_{\max}$), while in LMMF it is 5.5 Gbps. This is due to the maximization capacity optimization in the LMMCF scheme.

Figure 7 explains the bit rate fairness among the nodes versus the visibility for different networks. The maximum fairness is $F = 1$ at $V \geq 3.4$ km for all topologies. The proposed schemes improve the fairness and outperform the P-L network, especially at low visibilities. Also, as expected, at specified visibility values, LMMF performs better than LMMCF. Specifically, at $V = 1.8$ km, the fairness is 1 for both F-L and LMMF, 0.85 for both LMMCF and P-L, and 0.55 for D-L.

Figure 8 indicates the average bit-error rate of the networks. Clearly, the LMMF/LMMFC and D-L topologies have nearly the same performance, and the average bit-error rates are between $10^{-5}$ and $10^{-4}$ ($\leq \mathrm{BER}_{\max}$) for a wide range of visibility. However, both F-L and P-L outperform the proposed topologies at all visibility values. This is because both LMMF and LMMFC give optimization priority for bit rate fairness and capacity, respectively, over the optimization of bit-error rate. Moreover, the average bit-error rates for both the F-L and P-L networks are strongly affected by atmospheric visibility because there is no resource sharing among different nodes in the networks.

Figure 9 shows the effect of operating optical wavelength on both reliability and capacity of the LMMCF network at different visibilities. Clearly, the 1550 nm FSO link achieves higher reliability and capacity than that of the 780 nm FSO link. Specifically, at $V = 1.4$ km, the LMMCF network operating at 1550 nm drops two nodes only, while that operating at 780 nm drops four nodes. In addition, at this visibility, the network achieves capacities of 9 and 7.5 Gbps at 1550 and 780 nm, respectively. Generally, shorter wavelengths suffer from higher attenuation when propagating in an FSO channel.

The impacts of rainy weather on the performance of the networks considered are demonstrated in Figs. 10 and 11. Figure 10 shows network reliability in terms of number of dropped nodes versus rainfall rate $D$. Clearly, for all values of rainfall rate and with the same number of implemented

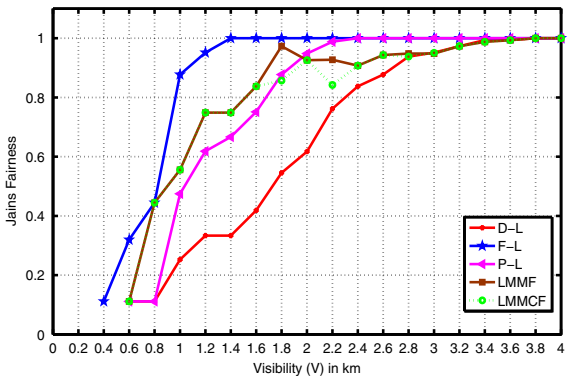


Fig. 7. Jain's bit rate fairness ($F$) versus visibility ($V$) for D-L, F-L, P-L, LMMF, and LMMCF networks.

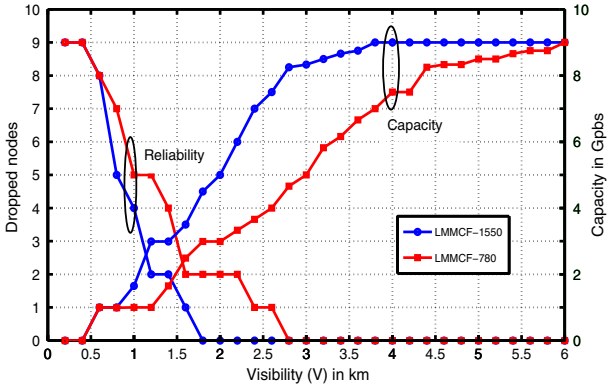


Fig. 9. Reliability and capacity of the LMMF scheme at two different operating wavelengths, 1550 and 780 nm, versus visibility ($V$).

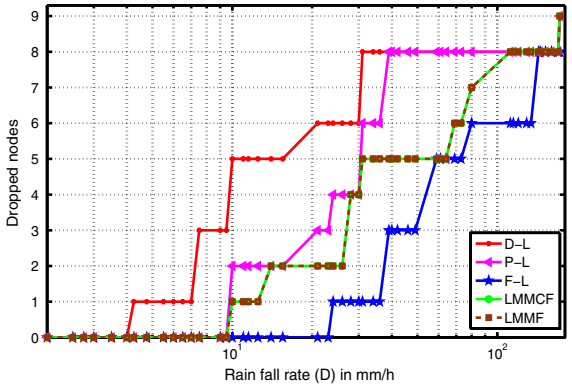


Fig. 10. Reliability versus the rain fall rate ($D$) for D-L, F-L, P-L, LMMF, and LMMCF networks.

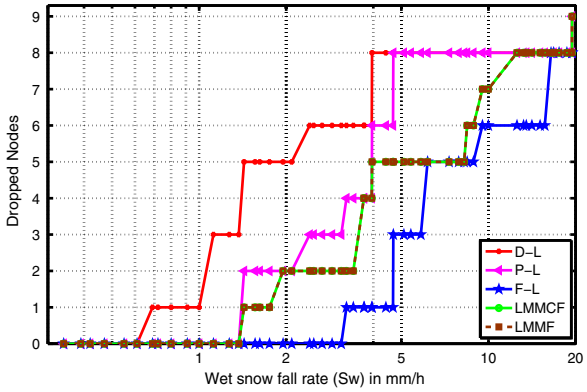


Fig. 12. Reliability versus wet snow fall rate ($S_w$) for D-L, F-L, P-L, LMMF, and LMMCF networks.

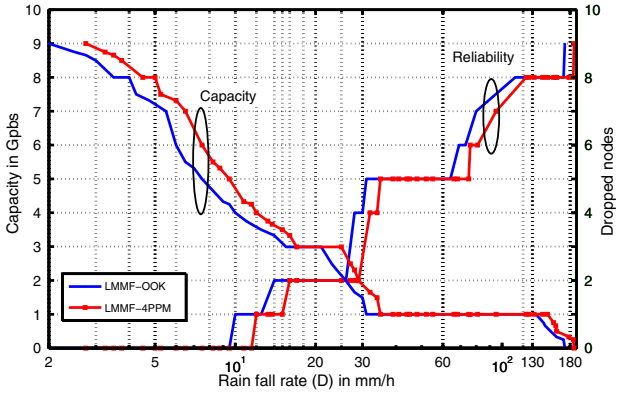


Fig. 11. Reliability and capacity of LMMF scheme for OOK and 4-PPM modulation versus rain fall rate ($D$).

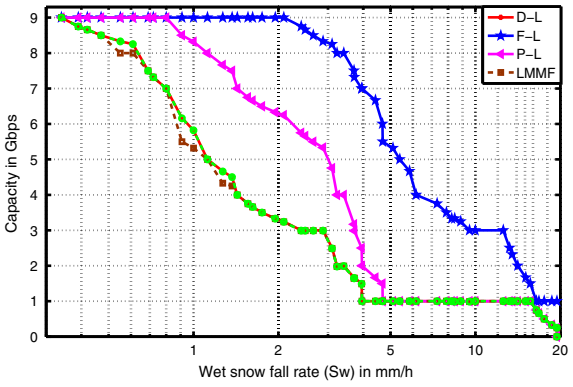


Fig. 13. Capacity versus wet snow fall rate ($S_w$) for D-L, F-L, P-L, LMMF, and LMMCF networks.

optical transceivers, both the LMMF and LMMCF schemes have higher reliability than the P-L scheme. Numerically, at $D = 10$ mm/h, five, two, and one node(s) are dropped in the D-L, P-L, and LMMF/LMMCF networks, respectively. In addition, Fig. 11 explains the modulation impact on LMMF scheme performance, where there are remarkable improvements in network reliability and capacity performance for 4-PPM (2 bits/frame) over NR-OOK at the same average transmitted power and background noise. Numerically, at $D = 30$ mm/h, the network drops three and five nodes for 4-PMM and NR-OOK, respectively. Also, at $D = 10$ mm/h, the capacities are 4 Gbps and 5 Gbps for 4-PMM and NR-OOK, respectively. Clearly, PPM has higher immunity against severe weather conditions over the OOK format, which enables the direct link to survive and hence increase network capacity. Reference [11] shows the rest of the results for rainy channels for the networks considered.

Figures 12–15 demonstrate wet snow impacts on the performance of the networks considered. Figure 12 explains the reliability versus snow fall rate $S_w$. Specifically, at $S_w = 10$ mm/h, eight, seven, and six nodes are dropped in the D-L/P-L, LMMF/LMMCF, and F-L models, respectively.

Moreover, on the one hand, as indicated in Fig. 13, the F-L network maintains $C = 9$ Gbps until $S_w = 2$ mm/h,

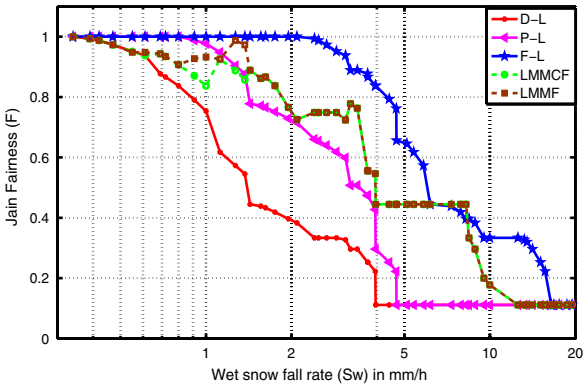


Fig. 14. Fairness ($F$) versus wet snow fall rate ($S_w$) for D-L, F-L, P-L, LMMF, and LMMCF networks.

and with a severe atmosphere, $S_w = 20$ mm/h, F-L still maintains about $C = 1$ Gbps. However, as expected, at different $S_w$ values, the performance of LMMCF is better than that of the LMMF scheme. On the other hand, Fig. 14 shows the bit rate fairness among the nodes versus $S_w$, where the P-L network maintains $F = 1$ until

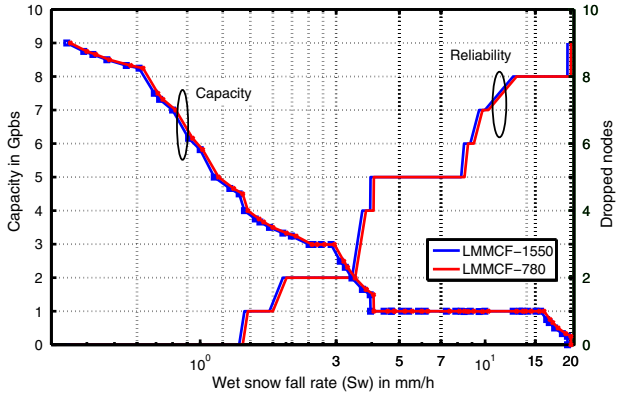


Fig. 15. Reliability and capacity of LMMCF scheme at two different wavelengths, 1550 and 780 nm, versus wet snow fall rate ($S_w$).

$S_w = 1$ mm/h and outperforms the proposed schemes, while, with a worse atmosphere of $S_w \geq 1.5$ mm/h, both LMMF then LMMCF achieve better fairness performance than the P-L topology. In addition, as indicated in Fig. 15 for the LMMCF scheme, insignificant enhancements are achieved in both network reliability and capacity for the 780 nm FSO link over the 1550 nm FSO link. Particularly, the first node is dropped at $S_w = 1.43$ mm/h and $S_w = 1.47$ mm/h for the 1550 and 780 nm FSO links, respectively.

The impacts of dry snow weather on the performance of the networks considered are demonstrated in Fig. 16. Figure 16 shows that, at $S_d = 2.5$ mm/h, the number of dropped nodes for the D-L/P-L, LMMF/LMMCF, and F-L networks are eight, five, and three nodes, respectively. The details of impacts for dry snow weather on the performance of the networks considered are demonstrated in [10].

Generally, the previous results show that the LMMCF/LMMF schemes offer better performance in reliability and fairness in different weather conditions at lower network cost. Further improvement could be achieved by using appropriate wavelength and modulation schemes. Also, the impact of dry snow is the strongest over both wet snow and rain at the same fall rate. Precisely, the considered networks are completely dropped at $S_d = 9$ mm/h, $S_w = 20$ mm/h, and $D = 180$ mm/h as shown in Figs. 16, 12, and 10, respectively.

Figures 17 and 18 compare the performance of the LMMCF and LMMF schemes, respectively, under both fixed and adaptive transmitted powers. For the fixed power scheme, the transmitted power is $P \in \{0, -15\}$ dBm, while for the adaptive power scheme, the transmitted power is $P \in \{0, -18, -17, -16.5, -16, -15.5, -15\}$ dBm. Clearly, as indicated in these figures, adaptive power schemes achieve much higher power efficiency than that of the fixed ones in both the LMMCF and LMMF schemes. Clearly, this comes with the price of increasing the average bit-error rate in the network. Numerically, for the LMMCF scheme with foggy weather as indicated in Fig. 17, at $V = 2$ km, the average transmitted powers for cases of adaptive power and fixed power are –8 and –5 dBm, respectively. Also, at this visibility value, the average error rates for the adaptive power and fixed power schemes are $0.5 \times 10^{-4}$ and $1^{-5}$, respectively. Figure 18 shows the same behavior for the LMMF scheme under rainy weather conditions.

Figures 19 and 20 indicate the performance difference between the lexicographic and weighted sum schemes, and in our case all schemes achieved the same reliability

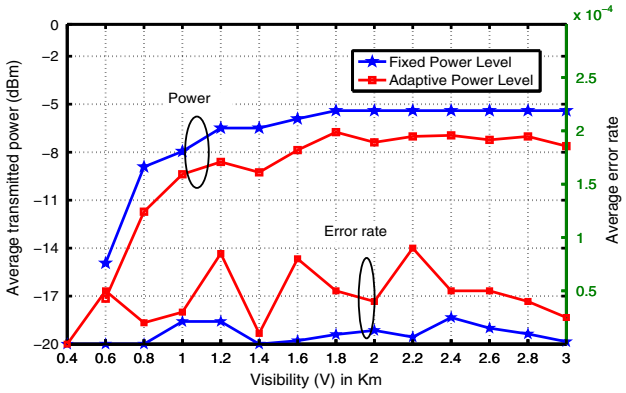


Fig. 17. Average transmitted power and average error rate for fixed and adaptive power LMMCF schemes in a foggy channel.

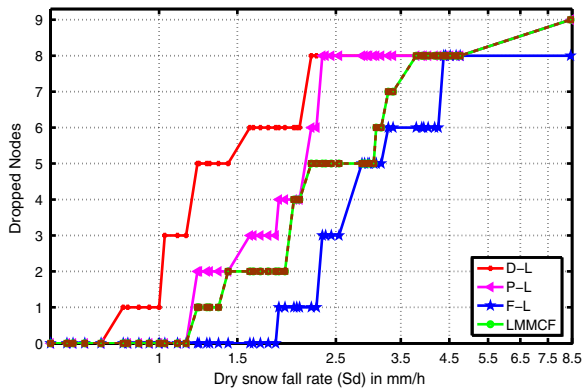


Fig. 16. Reliability versus dry snow fall rate ($S_d$) for D-L, F-L, P-L, LMMF, and LMMCF networks.

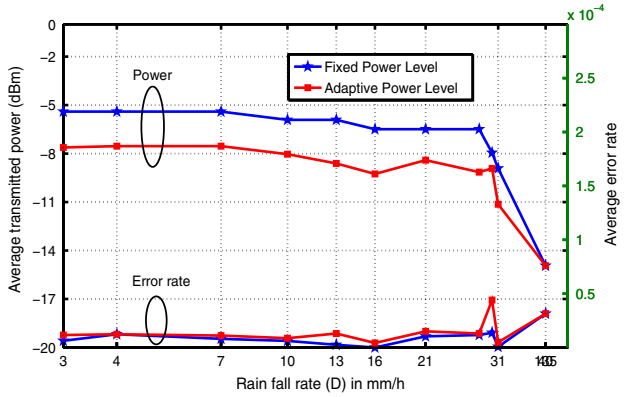


Fig. 18. Average transmitted power and average error rate for fixed and adaptive power LMMF schemes in a rainy channel.

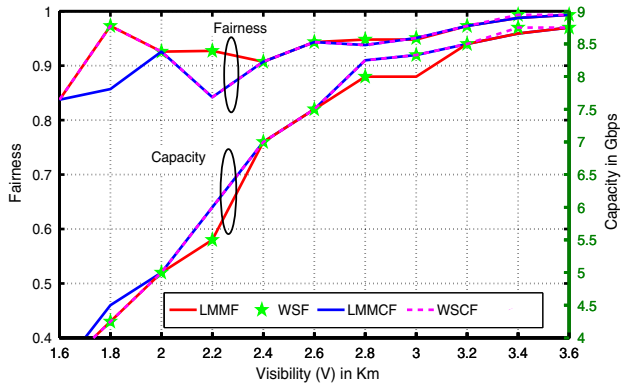


Fig. 19. Capacity and fairness versus the visibility ($V$) for lexicographic and weighted sum schemes.

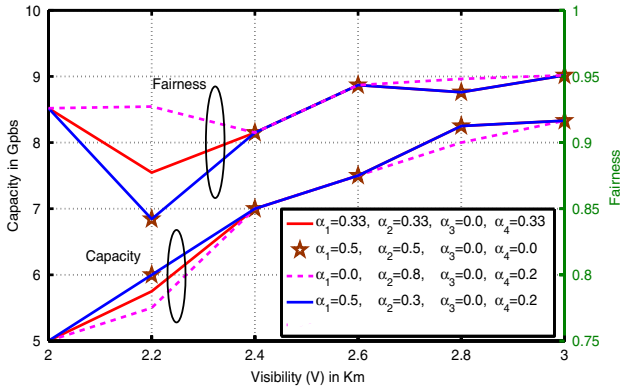


Fig. 20. Capacity and fairness versus visibility ($V$) for different $\alpha_{ii}$ coefficients for weighted sum schemes.

performance for a foggy channel, as shown in Fig. 5. The formulations of the WSCF and WSF schemes are selected to be comparable to LMMCF and LMMF, respectively, where in WSCF the selected weights are $\alpha_1 = 0.5$, $\alpha_2 = 0.3$, and $\alpha_4 = 0.2$, while in WSF the selected weights are $\alpha_1 = 0$, $\alpha_2 = 0.8$, and $\alpha_4 = 0.2$ ($\alpha_3 = 0$ for fixed power links). As indicated by Fig. 19, LMMCF always achieves the highest capacity over the entire visibility range. Also, WSCF achieves higher capacity than that of the LMMF and WSF schemes. On the other hand, Fig. 20 indicates the superior performance of both LMMF and WSF in terms of bit rate fairness compared to other schemes. However, the performance of the WSCF and WSF schemes is strongly affected by the selected value of the optimization weights. Clearly, as indicated in Fig. 20, an increase of weight $\alpha_1$ results in significant enhancement in network capacity associated with an inherent decrease in the bit rate fairness among the different nodes.

Last, it is worth noting that both reliability and bit rate fairness of the dynamic cooperative FSO network could be significantly enhanced by allocating more optical transceivers to the nodes near the backbone node. Clearly, these nodes have less distance to the central node and their direct FSO links have better qualities in severe weather conditions. However, the optimal transceiver distribution(s) [optimal transceiver placement(s)] $Z_k$ is out of the scope of this paper and could be investigated in future research work to obtain the optimal transceiver distribution in reconfigurable cooperative FSO networks.

## VI. Conclusion

Two resource allocation schemes have been proposed to improve both the reliability and fairness of dynamic cooperative FSO networks. One of these schemes enhances the network capacity over the bit rate fairness and the other does the opposite. The proposed schemes have assumed that the outer nodes have one optical transceiver, while the inner nodes are equipped with two transceivers. Each scheme is formulated as a discrete linear multi-objective optimization problem (ILP-MOP). Both schemes are evaluated and compared to relayed networks (partial and full relayed) under different weather conditions, e.g., fog, rain, and snow. Using the same number of optical transceivers, our results reveal that the proposed schemes achieve better reliability and bit rate fairness over partial relayed networks at all weather conditions. In addition, the results indicate that the impact of dry snow droplets on network performance is higher than both wet snow and rain droplets at the same fall rate. As future research, the network performance could be evaluated for different allocations of additional optical transceivers on different nodes, and the optimal distribution of these transceivers could be obtained.

## Acknowledgment

This work is supported by the Ministry of Higher Education (MoHE) of Egypt and is funded by an STDF grant #12670, Science and Technology Development Fund, Egypt.

## References

[1] I. I. Kim, B. McArthur, and E. J. Korevaar, "Comparison of laser beam propagation at 785 nm and 1550 nm in fog and haze for optical wireless communications," *Proc. SPIE*, vol. 4214, pp. 26–37, 2001.

[2] H. H. Refai, J. J. Sluss, H. H. Refai, and M. Atiquzzaman, "Comparative study of the performance of analog fiber optic links versus free-space optical links," *Opt. Eng.*, vol. 45, no. 2, 025003, 2006.

[3] S. Bloom, E. Korevaar, J. Schuster, and H. Willebrand, "Understanding the performance of free-space optics [Invited]," *J. Opt. Netw.*, vol. 2, no. 6, pp. 178–200, 2003.

[4] "Prediction methods required for the design of terrestrial free-space optical links," ITU-R Recommendation P.1814, 2007.

[5] A. Vavoulas, H. G. Sandalidis, and D. Varoutas, "Weather effects on FSO network connectivity," *J. Opt. Commun. Netw.*, vol. 4, no. 10, pp. 734–740, 2012.

[6] M. A. Kashani, M. Safari, and M. Uysal, "Optimal relay placement and diversity analysis of relay-assisted free-space optical communication systems," *J. Opt. Commun. Netw.*, vol. 5, no. 1, pp. 37–47, 2013.

[7] Z. Hu, P. Verma, and J. Sluss, Jr., "Improved reliability of free-space optical mesh networks through topology design," *J. Opt. Netw.*, vol. 7, no. 5, pp. 436–448, 2008.

[8] S. D. Milner, T.-H. Ho, I. I. Smolyaninov, S. Trisno, and C. C. Davis, "Free-space optical wireless links with topology control," *Proc. SPIE*, vol. 4821, pp. 175–180, 2002.

[9] A. S. Ghazy, H. A. I. Selmy, and H. M. H. Shalaby, "Fair cooperative resource allocation schemes for foggy free space optical network," in *Int. Conf. on Transparent Optical Networks (ICTON)*, 2015, vol. 2, pp. 178–200.

[10] A. S. Ghazy, H. A. I. Selmy, and H. M. H. Shalaby, "Reliable-fair resource allocation schemes for snowy cooperative free space optical networks," in *Asia Communications and Photonics Conf. (ACP)*, 2015, vol. 3, pp. 278–300.

[11] A. S. Ghazy, H. A. I. Selmy, and H. M. H. Shalaby, "Proposed resource allocation schemes for rainy free space optical network," in *Proc. 4th Int. Conf. on Photonics, Optics and Laser Technology*, 2016, pp. 74–81.

[12] R. M. Gagliardi and S. Karp, *Optical Communications*, 2nd ed. New York: Wiley, 1995.

[13] J. H. Churnside, "Aperture averaging of optical scintillations in the turbulent atmosphere," *Appl. Opt.*, vol. 30, no. 15, pp. 1982–1994, 1991.

[14] L. C. Andrews, R. L. Phillips, and C. Y. Hopen, *Laser Beam Scintillation With Applications*. Bellingham, WA: SPIE, 2001, vol. 99.

[15] L. C. Andrews and R. L. Phillips, *Laser Beam Propagation Through Random Media*. Bellingham, WA: SPIE, 2005, vol. 52.

[16] M. A. Khalighi and M. Uysal, "Survey on free space optical communication: A communication theory perspective," *IEEE Commun. Surv. Tutorials*, vol. 16, no. 4, pp. 2231–2258, 2014.

[17] O. Barsimantov and V. V. Nikulin, "Adaptive optimization of a free space laser communication system under dynamic link attenuation," *J. Opt. Commun. Netw.*, vol. 3, no. 3, pp. 215–222, 2011.

[18] P. T. Dat, A. Bekkali, K. Kazaura, K. Wakamori, and M. Matsumoto, "A universal platform for ubiquitous wireless communications using radio over FSO system," *J. Lightwave Technol.*, vol. 28, no. 16, pp. 2258–2267, 2010.

[19] R. T. Marler and J. S. Arora, "Survey of multi-objective optimization methods for engineering," *Struct. Multidiscip. Optim.*, vol. 26, no. 6, pp. 369–395, 2004.

[20] H. Isermann, "Linear lexicographic optimization," *OR Spectrum*, vol. 4, no. 4, pp. 223–228, 1982.

[21] W. Ogryczak and T. Sliwinski, "Lexicographic max-min optimization for efficient and fair bandwidth allocation," in *Int. Network Optimization Conf. (INOC)*, 2007.

[22] W. Ogryczak and T. Sliwinski, "On direct methods for lexicographic min-max optimization," in *Computational Science and Its Applications (ICCSA)*, 2006, pp. 802–811.

[23] R. Jain, D. Chiu, and W. Hawe, "A quantitative measure of fairness and discrimination for resource allocation in shared computer systems," arXiv:cs/9809099, 1998.

[24] C. Paar and J. Pelzl, *Understanding Cryptography: A Textbook for Students and Practitioners*. New York: Springer, 2009.

[25] D. E. Golberg, *Genetic Algorithms in Search, Optimization, and Machine Learning*. Boston: Addison-Wesley, 1989.

**Abdallah S. Ghazy** was born in Giza, Egypt, in 1983. He received the B.S. degree from Azher University, Egypt, in 2007 in electrical engineering. He worked in voice-data systems in Telecom-Egypt and AVAYA-Egypt for six years, from 2008 to 2013. In 2012, he joined the Electronics and Electrical Communications Engineering Department, Azher University, Egypt. He is currently on leave from Azher University and is working toward the M.S. degree at Egypt-Japan University of Science and Technology, Alexandria, Egypt. His research interests include optical communication, wireless communication, and heterogeneous communication networks.

**Hossam A. I. Selmy** was born in Giza, Egypt, in 1979. He received the B.S. and M.S. degrees from Cairo University, Egypt, in 2001 and 2007, respectively, and the Ph.D. degree from Egypt-Japan University for Science and Technology, Egypt, in 2013, all in electrical engineering. He is currently an Assistant Professor at the National Institute of Laser Enhanced Science (NILES), Cairo University. His research interests include advanced modulation and multiple access schemes for optical fiber communication and next-generation wireless access networks.

**Hossam M. H. Shalaby** (S'83–M'91–SM'99) was born in Giza, Egypt, in 1961. He received the B.S. and M.S. degrees from Alexandria University, Alexandria, Egypt, in 1983 and 1986, respectively, and the Ph.D. degree from the University of Maryland at College Park in 1991, all in electrical engineering. In 1991, he joined the Electrical Engineering Department, Alexandria University, and was promoted to Professor in 2001. From September 2010 to August 2016, he was the Chair of the Department of Electronics and Communications Engineering, Egypt-Japan University of Science and Technology (E-JUST), Alexandria, Egypt. From September 1996 to January 1998, he was with the Electrical and Computer Engineering Department, International Islamic University Malaysia, and from February 1998 to February 2001, he was with the School of Electrical and Electronic Engineering, Nanyang Technological University, Singapore. His research interests include optical communication, silicon photonics, optical space-division multiplexing, optical CDMA, and information theory. He is a senior member of the IEEE Photonics Society and The Optical Society (OSA).